JGR Atmospheres

RESEARCH ARTICLE
10.1029/2025JD045524

Deforestation Impacts on Clouds and Precipitation Over Borneo Vary Across the Diurnal Cycle

G. Leung[1,2] **and S. C. van den Heever**[1]

[1]Department of Atmospheric Science, Colorado State University, Fort Collins, CO, USA, [2]Department of Atmospheric and Oceanic Sciences, University of Wisconsin—Madison, Madison, WI, USA

Key Points:

- Vegetation shifts following deforestation lower sensible heating and raise latent heating as evapotranspiration offsets surface warming
- Deforestation decreases shallow cloud cover but enhances cloudiness along deforestation boundaries via vegetation breezes
- Deforestation weakens the moisture convergence driving sea breeze deep convective rainfall but shallow cumuli rain earlier in the day

Supporting Information:

Supporting Information may be found in the online version of this article.

Correspondence to:

G. Leung,
bee.leung@wisc.edu

Citation:

Leung, G., & van den Heever, S. C. (2026). Deforestation impacts on clouds and precipitation over Borneo vary across the diurnal cycle. *Journal of Geophysical Research: Atmospheres*, *131*, e2025JD045524. https://doi.org/10.1029/2025JD045524

Received 26 SEP 2025
Accepted 14 MAR 2026

Author Contributions:

Conceptualization: G. Leung, S. C. van den Heever
Formal analysis: G. Leung
Funding acquisition: G. Leung, S. C. van den Heever
Methodology: G. Leung
Resources: S. C. van den Heever
Software: G. Leung
Supervision: S. C. van den Heever
Visualization: G. Leung
Writing – original draft: G. Leung
Writing – review & editing: S. C. van den Heever

Abstract The impact of tropical deforestation on clouds and precipitation remains uncertain due to complex interactions between land and atmospheric processes on convective and mesoscales. Here, we examine convective-scale processes controlling the short-term atmospheric response to deforestation over Borneo using multi-day large eddy simulations. Replacing tropical forests with oil palm plantations reduces surface roughness, leading to less efficient surface–atmosphere exchange, warmer soils, and a cooler but moister near-surface atmosphere. To examine how this impacts cloud formation, we identify and track thousands of clouds to quantify shifts in tropical convection across the diurnal cycle. Overall, deforestation suppresses shallow-to-deep convective development, though the shallow cumuli which do form start lightly raining earlier in the day due to increased low-level moisture. However, this reduction in shallow cloud cover is not spatially uniform: in areas where the deforestation gradient is strong, midday cumuli are enhanced by mesoscale vegetation breezes. Deforestation also weakens sea breeze-driven moisture convergence, leading to the relative enhancement of terminal congestus over deep convection and a shift in precipitation onset toward later in the evening. Our findings emphasize that deforestation impacts vary diurnally depending on cloud type and interactions with mesoscale phenomena, as well as spatially depending on the location relative to deforested regions. Although this work focuses on the transient convective response to deforestation, we suggest the multi-scale variability of these responses should be considered when assessing longer-term deforestation impacts on clouds, rain, and climate.

Plain Language Summary Deforestation is widespread in the tropics. Though we know that changes to the land surface can impact the atmosphere above it, we still do not fully understand how these changes affect different types of clouds throughout the day. Here, we use an atmospheric model to simulate clouds over Southeast Asia. We explore how deforestation impacts cloud formation by comparing simulations with the same atmospheric conditions but using pre- and post-deforestation land cover. Most crucially, we find that deforestation can have contrasting impacts on cloudiness depending on the time of day and spatial scale. Deforestation slows the transition of shallow clouds into deep convection. However, it locally increases cloudiness close to the deforestation boundary by driving breezes between the forest and deforested areas. The impacts of deforestation on rainfall are similarly complex, with increases in areas covered by weak rain but a large decrease in rainfall amounts overall. These findings show that the impact of deforestation on clouds and rainfall is not simple. The atmospheric response to forest loss depends on many competing processes that need to be considered if we want to accurately predict how deforestation impacts freshwater availability, precipitation extremes, and the climate and hydrology of tropical regions.

1. Introduction

Anthropogenic activities drive widespread deforestation in the tropics (Kim et al., 2015; Winkler et al., 2021). Southeast Asia—particularly Borneo—is a hotspot of tropical deforestation, with extensive forest clearing in recent decades driven primarily by oil palm and rubber plantations (S. Chen et al., 2024; Jamaludin et al., 2022; Parker et al., 2024). Changes in land surface properties are known to impact the atmosphere through altering fluxes of heat, moisture, and momentum (Mahmood et al., 2014; Santanello et al., 2018). However, how this translates to impacts on clouds and rainfall remains uncertain (Gentine et al., 2019).

Changes in land surface properties drive changes in the surface energy budget, which in turn drive boundary layer moisture and temperature responses. First, deforestation potentially leads to local low-level warming and drying, which have opposite impacts on convection. Moreover, the atmospheric circulations may respond to these local

changes, for example, by enhancing moisture convergence and thus convection (C.-C. Chen et al., 2019). The net impact of these contrasting feedbacks appears to depend on the background meteorology (Findell & Eltahir, 2003) and cloud type (Baidya Roy & Avissar, 2002; Cioni & Hohenegger, 2017). Changes in clouds caused by land cover changes in turn feed back onto the surface energy budget. These interactions between the surface and convection further complicate the cloud response to deforestation, particularly since this land-atmosphere coupling evolves on diurnal timescales.

Recent satellite-based estimates suggest that deforestation in Southeast Asia locally enhances cloud cover (Leung et al., 2024; Xu et al., 2022), though the magnitude of the response depends on meteorology and time of day. Although such observational quantifications are essential, it is challenging to elucidate the mechanisms driving cloud responses from these long-term estimates. Observations must be complemented with process-oriented modeling studies.

Most modeling-based investigations of deforestation impacts over Southeast Asia have used global or regional climate models over long integration times (C.-C. Chen et al., 2019; H.-Chen & Lo, 2023; Schneck & Mosbrugger, 2011; Takahashi et al., 2017; Tölle et al., 2017; Werth & Avissar, 2005). However, disagreements remain about the sign of deforestation impacts on cloudiness. This is perhaps to be expected, given that convective processes are not explicitly resolved in large-scale models and are thus sensitive to how models parameterize convective responses to compensating local thermodynamic changes. The convective response to deforestation may be sensitive to the mean-state climate owing to model and parameterization differences (H.-Chen & Lo, 2023). This uncertainty highlights the need to improve our understanding of land surface–convection interactions at scales where convective processes can be more accurately resolved, especially in regions like Southeast Asia where most convection is driven by diurnally reversing mesoscale flows (e.g., sea breezes, terrain flows) that are sensitive to surface properties (Qian, 2008; Yang & Slingo, 2001).

Despite these challenges in quantifying cloud responses to forest loss, doing so is essential to characterizing deforestation impacts on weather, hydrology, and the Earth's energy balance (Boysen et al., 2020; Laguë et al., 2021). Such impacts may vary between different types of convection (Gentine et al., 2019). Thus, we must understand how different cloud types and associated precipitation rates respond to changes in the land surface.

This research aims to quantify deforestation impacts on a range of tropical convection, as well as to elucidate the convective and meso-scale processes driving these impacts. We address the following science questions: (a) how does deforestation impact different cloud types across the diurnal cycle? and (b) what is the impact of those cloud responses on surface precipitation? We address these questions by tracking clouds in a pair of high-resolution simulations with forested and deforested land cover (Section 2). We quantify how land surface changes impact the surface energy budget and near-surface atmosphere (Section 3), then discuss cloud (Section 4) and precipitation responses (Section 5) to deforestation across the diurnal cycle. Finally, we summarize our findings and discuss broader implications (Section 6).

2. Methods

2.1. Model Description and Configuration

We conducted large eddy simulations (LES) using the Regional Atmospheric Modeling System (RAMS v6.3.04) (Cotton et al., 2003; Pielke Sr. et al., 1992; Saleeby & van den Heever, 2013). Full model settings are provided in Table 1, but we describe key aspects of the simulation design below.

Our simulations reproduce the diurnal cycle of convection (Figure 1), including the daytime transition from shallow to deep convection during synoptically benign conditions, when convection is primarily driven by local thermodynamics rather than large-scale forcing. The simulation domain (Figure 2) encompasses a large area (~322 × 334 km) in northwestern Borneo, which experienced extensive land cover changes in past decades (Section 2.2). The morphology, timing, and distribution of clouds in our simulations are similar to observations (Figure 1). However, we emphasize that we analyze these simulations in a statistical manner to examine land-convection interactions in the region, rather than as a case study recreating a specific day's meteorology.

Table 1
RAMS Parameters

Model aspect	Description
Grid	Arakawa-C grid
	2,150 × 2,230 points, $\Delta x = \Delta y = 150$ m
	106 vertical levels, $\Delta z = 50$–300 m with a stretch ratio of 1.04
Timestep	$\Delta t = 1.5$s
	Output every 5 min
Integration time	6 hr spin-up time (excluded from analysis) + 72 hr (3 diurnal cycles)
Initialization	Initialized from ERA-5 (Hersbach et al., 2020)
Boundary conditions	Nudged with hourly ERA-5 data at lateral (25 grid points from side) and top (above 22 km) boundaries with nudging timescale = 900s (15 min)
Surface scheme	Land Ecosystem-Atmosphere Feedback (LEAF-3) (Walko et al., 2000)
	Land cover taken from HILDA+ (Winkler et al., 2021) matched to LEAF-3 land cover classes
	Soil classes taken from UN FAO data set (FAO United Nations, 1974)
	11 soil layers extending to 0.5 m below the surface, with soil moisture and temperature initialized from ERA-5
Turbulence scheme	Smagorinsky (1963) with modifications from Lilly (1962) and Hill (1974)
Microphysics scheme	RAMS two-moment bin-emulating microphysics (Meyers et al., 1997; Saleeby & Cotton, 2008)
Radiation scheme	RTE-RRTMGP (Pincus et al., 2019)
	Radiation tendencies updated every 5 min
Aerosol treatment	Aerosol number concentration = 600 cm^{-3} at surface, exponentially decreasing with height with scale height of 7 km
	Fixed aerosol concentrations (no sources, sinks, or advection)
	Aerosol-radiation interactions are represented

To resolve the initiation and development of shallow cumuli, we used a fine spatiotemporal resolution ($\Delta x = \Delta y = 150$ m, $\Delta z = 50$–300 m, $\Delta t = 1.5$s). This, in combination with our large model domain integrated over three diurnal cycles (72 hr, 17–20 September 2019) allowed us to extensively sample tropical convection. We selected this year to coincide with measurements of cloud and aerosol properties in the region during the NASA CAMP^{2}Ex campaign (Reid et al., 2023). The specific simulation period was directly before the transition from southwest to northeast monsoon and captured a major biomass burning event, establishing a baseline for future planned experiments on aerosol modulation of deforestation impacts on convection.

We initialized and nudged the lateral boundary conditions using ERA-5 reanalysis (Hersbach et al., 2020), which constrained the synoptic scale environment while ensuring that convective and mesoscale features evolve freely in the domain. Two-way land-atmosphere exchanges were parameterized using the Land Ecosystem Atmosphere Feedback (LEAF-3) (Walko et al., 2000) surface model. LEAF-3 represents turbulent and radiative exchange between the soil/ground, vegetation, and a canopy layer, which then exchanges energy, water, and momentum with the lowest atmospheric layer.

2.2. Experiment Set-Up

We conducted two simulations constrained with the same atmospheric initial boundary conditions but different land cover. Using identical large-scale atmospheric forcing allowed us to compare how land-atmosphere interactions impact local convective development.

Land cover was taken from the Historic Land Dynamics Assessment+ (HILDA+) data set (Winkler et al., 2021; $\Delta x,y = 1$ km). HILDA + land cover classes do not directly correspond to LEAF-3, so we matched the two by comparing HILDA+ with observed MODIS land cover (Friedl et al., 2002) and default RAMS land cover.

We ran one simulation with land cover from 1960 (VEG1960) and one with land cover from 2019 (VEG2019) (Figure 2). Previous work used land cover scenarios that were totally deforested (e.g., Takahashi et al., 2017;

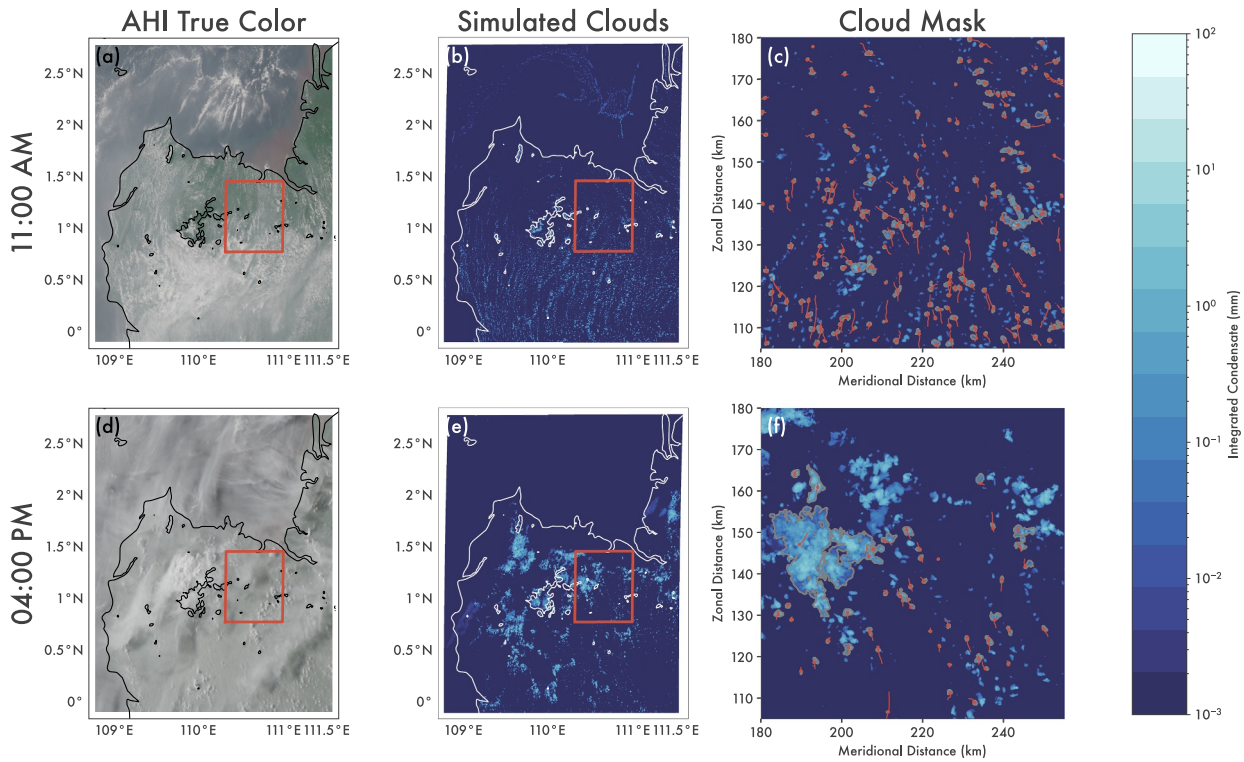

Figure 1. Simulations reproduce the observed diurnal cycle and distribution of convection, shown at 11:00a.m. (a–c) and 4:00p.m. (d–f) on 17 September 2019. Advanced Himawari Imager (AHI) true color (left) compared to VEG2019 integrated condensate (center). Solid contours show coastline and 500 m a.s.l. Red boxes (a, b, d, e) indicate regions in (c, f) demonstrating cloud tracking, with cloud centers (red circles), trajectories (red lines), and masks (gray contours).

Werth & Avissar, 2005) or idealized checkerboard-type patterns (e.g., Rieck et al., 2014); here, we examine the effects of realistic scales of deforestation and patterns of landscape heterogeneity.

The primary change between 1960 and 2019 is a widespread shift from "evergreen broadleaf forest" representing intact tropical rainforests to "wooded grassland" and "cropland" representing plantations of oil palm, rubber, and other agricultural uses. Unlike previous modeling studies examining deforestation in Southeast Asia that replace forest with C4-type grass (C.-C. Chen et al., 2019; Tölle et al., 2017), forest is primarily replaced by "wooded grassland" in our simulations. This surface type best matches observations of oil palm and rubber plantations in terms vegetation height (June et al., 2018) and evaporative resistance (Giambelluca et al., 2016). Transitions from tropical forest to palm oil and rubber plantations in Southeast Asia are unique in that they do not necessarily reduce evapotranspiration (Spracklen et al., 2018). Increases in "urban surface" are also evident. We refer to the combination of wooded grassland, cropland, and urban land cover types as "deforested." Compared to intact rainforests, deforested land has a lower surface roughness/shorter canopy height, larger albedo, and lower evaporative resistance (Figure 2).

2.3. Cloud Tracking

We tracked convective clouds using the Tracking and Object Based Analysis of Clouds (*tobac* v1.5) algorithm (Heikenfeld et al., 2019; Sokolowsky et al., 2024) (Figures 1c and 1f). A detailed description of our tracking approach can be found in Text S1 of Supporting Information S1. The large data set of identified clouds (>75,000 per simulation) allows for robust statistical assessment of a range of cloud modes, each of which may be coupled to the land surface via different processes.

3. Deforestation Impacts on the Domain Mean Surface Energy Budget (SEB)

We begin by examining the surface energy budget (SEB), diurnally averaged over land (Figure 3; Figure S1 in Supporting Information S1 shows averages by land cover). Though there is substantial spatial heterogeneity in

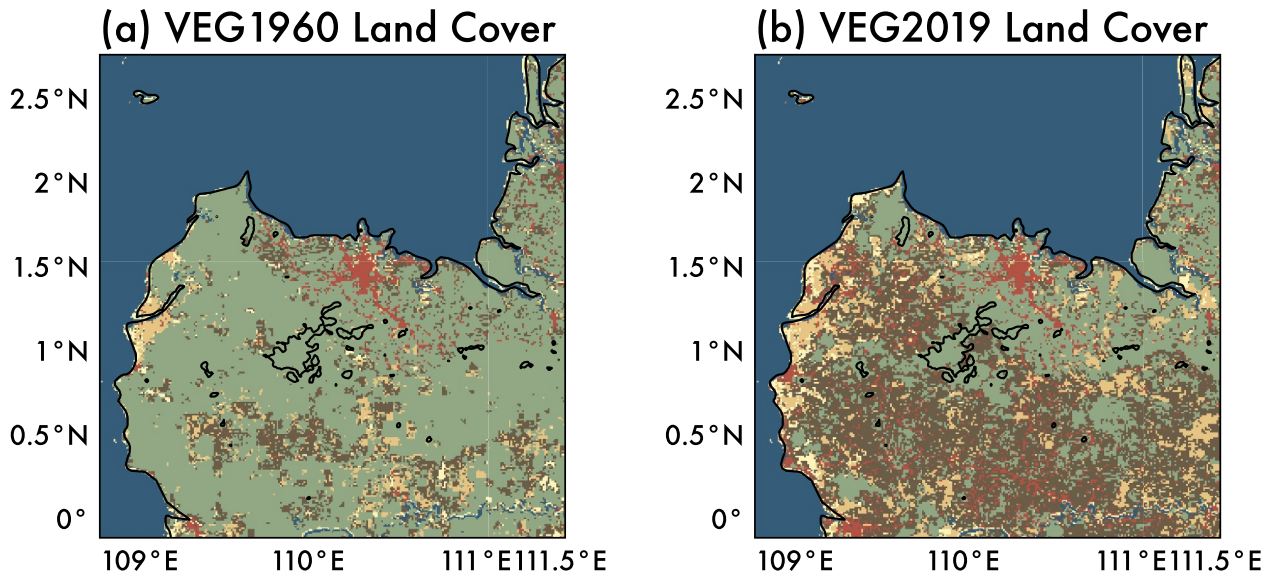

Land Cover Type	Vegetation Height (m)	Albedo	Min. Evaporative Resistance (s m^{-1})
Ocean	–	–	–
Evergreen broadleaf forest	32	0.15	500
Wooded grassland	7	0.18	100
Crop/mixed farming	1	0.18	100
Short grass	0.3	0.26	100
Urban	6	0.18	500

Figure 2. Model land cover set-up for (a) VEG1960 and (b) VEG2019. Contours show coastline and 500 m a.s.l. topography. Legend shows LEAF-3 land surface properties relevant to this study.

both the pattern of deforestation (Figure 2) and the atmospheric response, it is useful to first explore domain-means to understand the overall atmospheric response; we discuss the impacts of heterogeneous deforestation in Section 4.3 and 4.4.

The magnitude of radiative and turbulent fluxes in our simulations compare favorably with measurements over rainforests and oil palm plantations (Fowler et al., 2011; Takanashi et al., 2010; Tang et al., 2019). The magnitude of latent heat fluxes (LHF) is larger than that of sensible heat fluxes (SHF), due to the abundant moisture in the soil and vegetation canopy. The Bowen ratio ranges from 0.3 to 0.5 between 7 and 9a.m. (here and throughout, times are local time, UTC+8).

Deforestation from VEG1960 to VEG2019 (Figure 3a) drives robust SEB shifts (Figure 3b), with similar trends across simulation days. SEB changes across the simulations are dominated by SHF (red lines, Figure 3). Deforestation reduces energy transfer from the surface to the atmosphere via SHF (Figure S1c in Supporting Information S1). Compared to tall rainforests with high roughness lengths, the woody plantations are smoother and less efficient at transmitting energy into the atmosphere through turbulent fluxes.

Due to the inefficient turbulent exchange in deforested regions, more energy accumulates at the surface and heats the vegetation and ground (gray lines, Figure 3; Figure S1e in Supporting Information S1). We confirmed this by examining air in and above (~75 m a.g.l.) the canopy (Figure 4). The increased energy storage results in warmer land surface temperatures (Figure 4d), consistent with satellite (Crompton et al., 2021; Sabajo et al., 2017) and

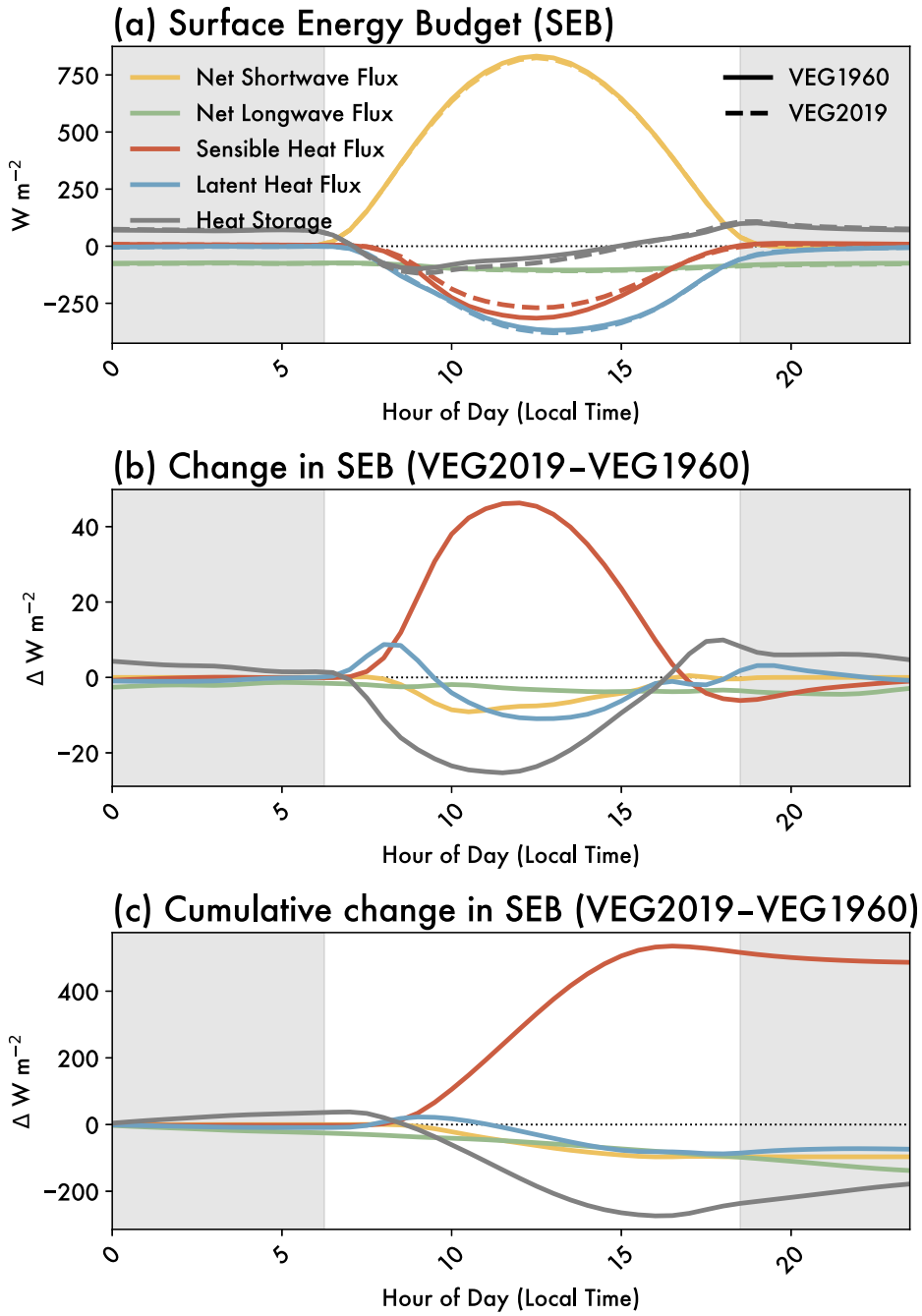

Figure 3. Diurnal evolution of the surface energy budget. (a) Mean surface energy budget averaged over land, where positive terms heat the surface and negative terms cool the surface. Solid lines represent VEG1960, and dashed lines represent VEG2019. (b) Difference and (c) cumulative difference between VEG2019 and VEG1960. Cumulative differences highlight relative contributions of each term to the integrated daily change. Gray shading shows nighttime.

field measurements (Hardwick et al., 2015). The warmer deforested surface radiates more energy as outgoing longwave radiation (OLR) (green lines, Figure 3c).

The warmer soil evaporates more and transfers more energy into the canopy in VEG2019. This enhances transpiration, with most energy stored in the canopy going toward latent heating. Deforested areas have lower evaporative resistance, meaning for a given temperature, they release more moisture into the atmosphere than forested regions. Deforestation thus moistens but only moderately warms canopy air (Figure 4e), despite the much

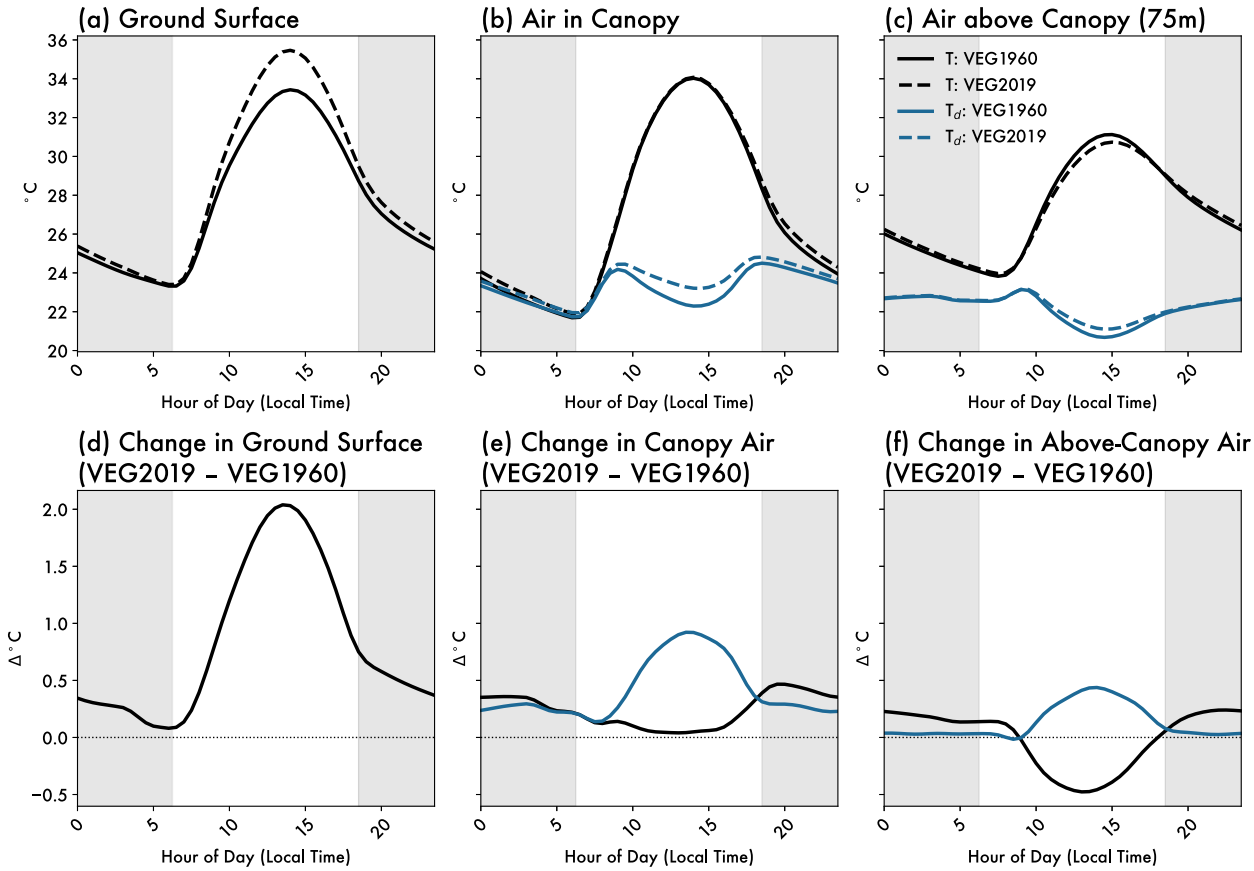

Figure 4. Diurnal evolution of (a) ground surface, (b) vegetation canopy air, and (c) air above canopy at 75 m a.g.l. for temperature (black) and dewpoint (blue), averaged over land. Solid lines represent VEG1960, and dashed lines represent VEG2019. VEG2019-VEG1960 differences for (d) ground surface, (e) canopy air and (f) above-canopy air.

warmer ground surface (Figure 4d). In situ measurements of canopy thermodynamic properties for this region are sparse, though Fowler et al. (2011) found that canopy temperatures in oil palms are slightly larger than in intact rainforests.

Turbulent exchange of energy and moisture between the canopy and above-canopy air is less efficient over the smoother deforested surface compared to the rougher forested one. The diurnal cycle of above-canopy air temperature and moisture is thus more modulated in VEG2019 than in VEG1960 (Figure 4c). This weakened vertical mixing leads to a moister low-level atmosphere in the deforested scenario after 9a.m. (blue lines, Figure 3; Figure S2 in Supporting Information S1). Secondarily, once the canopy heats up sufficiently, enhanced evapotranspiration (ET) in the deforested scenario contributes to low-level moistening, partially offsetting the effects of reduced vertical transport. The increase in LHF is consistent with in situ observations (Fowler et al., 2011; Giambelluca et al., 2016) and mesoscale modeling studies (van der Molen et al., 2006), but is opposite to past RCM/GCM studies in this region (C.-C. Chen et al., 2019; Takahashi et al., 2017; Tölle et al., 2017).

SEB responses to deforestation are primarily driven by surface roughness rather than albedo (Figure 3), as has been noted for the tropics (Davin & de Noblet-Ducoudré, 2010; Duveiller et al., 2021). We observe < 1% decrease in the magnitude of early morning (7–9a.m.) net shortwave (SW) flux following deforestation. Once clouds develop after 9a.m., there is a bigger deforestation impact on SW (yellow line; Figure 3). However, changes due to reduced cloud cover (more downwelling SW) and increased albedo (more upwelling SW) act in opposite directions, such that the SW contribution to surface energy budget changes is secondary to changes in SHF.

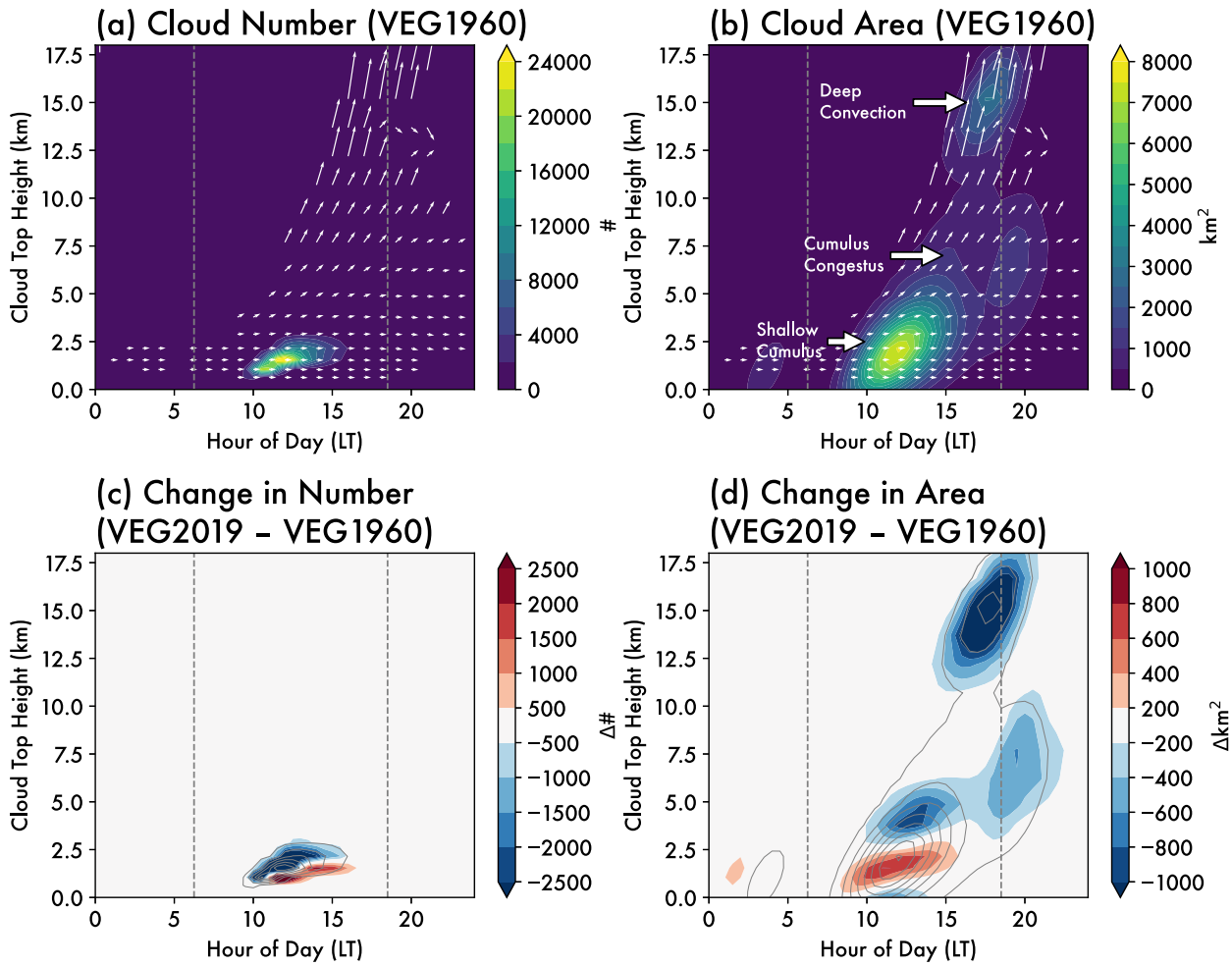

Figure 5. Diurnal cycle of total cloud number and area. Color contours show total (a) number and (b) area of *tobac*-tracked clouds for each joint hour-of-day and cloud top height (CTH) bin in VEG1960. White arrows indicate the mean CTH change over 5 min for a given (hour-of-day, CTH) bin. VEG2019-VEG1960 difference for cloud (c) number and (d) area, with gray contours from (a, b) for comparison. Gray vertical lines indicate sunrise and sunset.

4. Cloud Responses to Deforestation

4.1. Cloud Evolution

The mean diurnal cycle of convection (Figure 5) shows our simulations capture the trimodal convection distribution (Johnson et al., 1999) and shallow-to-deep convection transition (Argüeso et al., 2020; Marzuki et al., 2022; Renggono et al., 2001). *tobac*-tracked clouds are binned by CTH (5-model level intervals) and time-of-day (30-min intervals). We show cloud development as white arrows (Figures 5a and 5b); the horizontal component depicts a five-minute time interval, and the vertical component depicts the change in CTH over that interval, averaged over cells in a bin.

The surface heats up after sunrise (6:15a.m.) until shallow cumulus develops around 9a.m. These shallow cumuli (1 km < CTH < 3 km) are mostly non-precipitating. By 12p.m., the sea breeze propagates onshore, and congestus (4 km < CTH < 10 km) forms along the sea breeze convergence zone. These convective cells precipitate more strongly than those that develop earlier in the day, and produce cold pools that collide, creating low-level convergence. Some collisions result in deeper cumulonimbus (CTH > 10 km) from 4 to 6:30p.m., while other less favorably located congestus only reach maximum CTHs of ~8 km before dissipating. This division between congestus which eventually become deep convection (transient congestus) and those which do not (terminal congestus) (Luo et al., 2009; Leung & van den Heever, 2022) is evident as the bifurcation in the mean cloud development (white arrows; Figures 5a and 5b).

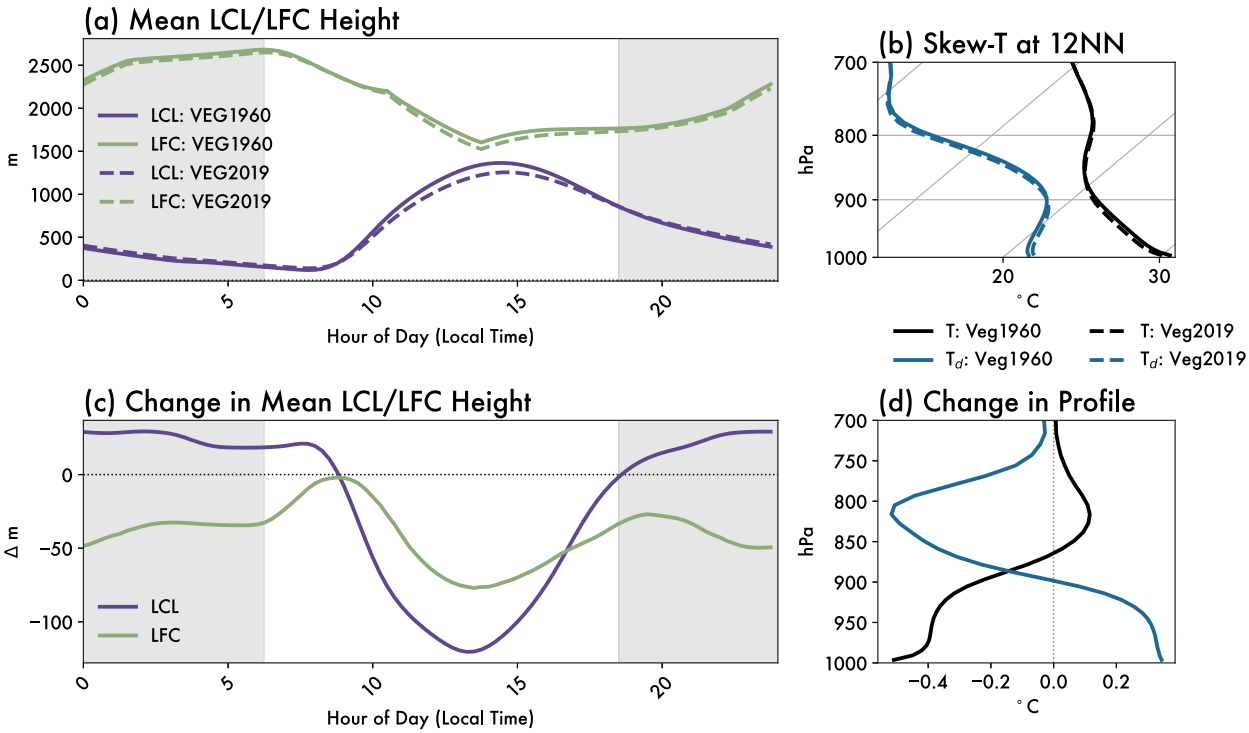

Figure 6. Diurnal evolution of lifted condensation level (LCL) and level of free convection (LFC), averaged over land. (a) LCL height in purple and LFC height in green. (b) Mean skew-T profile at 12p.m., with temperature (black) and dewpoint (blue). Solid lines represent VEG1960, and dashed lines represent VEG2019. VEG2019-VEG1960 difference for (c) LCL/LFC evolution and (d) atmospheric profile.

4.2. Mean Shallow Cloud Response

Deforestation-driven changes in surface–atmosphere interactions manifest as shifts in the cloud distribution (Figures 5c and 5d). Due to weaker SHFs (Figure 3), the planetary boundary layer (PBL) deepens more slowly in VEG2019 versus VEG1960. The lifted condensation level (LCL) is lower following deforestation (Figures 6a and 6c), meaning parcels lifted from the surface should form clouds at lower altitudes. However, weakened SHFs limit the ability of thermals to penetrate the LCL and form clouds. Deforestation thus shifts peak cloudiness later in the day (Figure 5c), once the PBL is sufficiently developed.

The cloud response to lower SHFs following deforestation is counteracted by increased evapotranspiration (Figure 3) and decreased vertical mixing over smooth deforested surfaces. This reduced vertical transport keeps moisture near the surface in the deforested scenario (Figures 6b and 6d). The lower LCL in VEG2019 coincides with an increased distance between the LCL and the level of free convection (LFC) around midday, meaning enhanced convective inhibition (Figures 6a and 6c). Even if parcels do reach the lower LCL, they are not positively buoyant and less likely to become active cumuli (Gentine et al., 2013; Stull, 1988).

4.3. Mesoscale Circulations and Deforestation Heterogeneity

Mesoscale circulations locally impact cloud frequency. Figure 7 shows the deforestation-driven change in the diurnal cycle amplitude. We calculate the mean cloud diurnal cycle based on the number of clouds in each 6×6 km box at each time of day (15-min increments). We tested other averaging windows in space (1.5–15 km) and time (5–60 min) and found qualitatively similar results; we selected these parameters for clear visualization. For each location, we find the diurnal peak in the number of clouds and compare this for VEG2019 and VEG1960. Figure 7 thus accounts for temporal offsets in the diurnal cycle (e.g., if cloud development peaks later/earlier). For most regions, there is a decrease in peak cloud number, consistent with our earlier findings that deforestation suppresses shallow cumuli (Figure 5c). However, there are some areas where cloudiness is enhanced following deforestation (red; Figure 7a). In these regions, midday cloud number and cloud fraction are greater following deforestation (Figure 7).

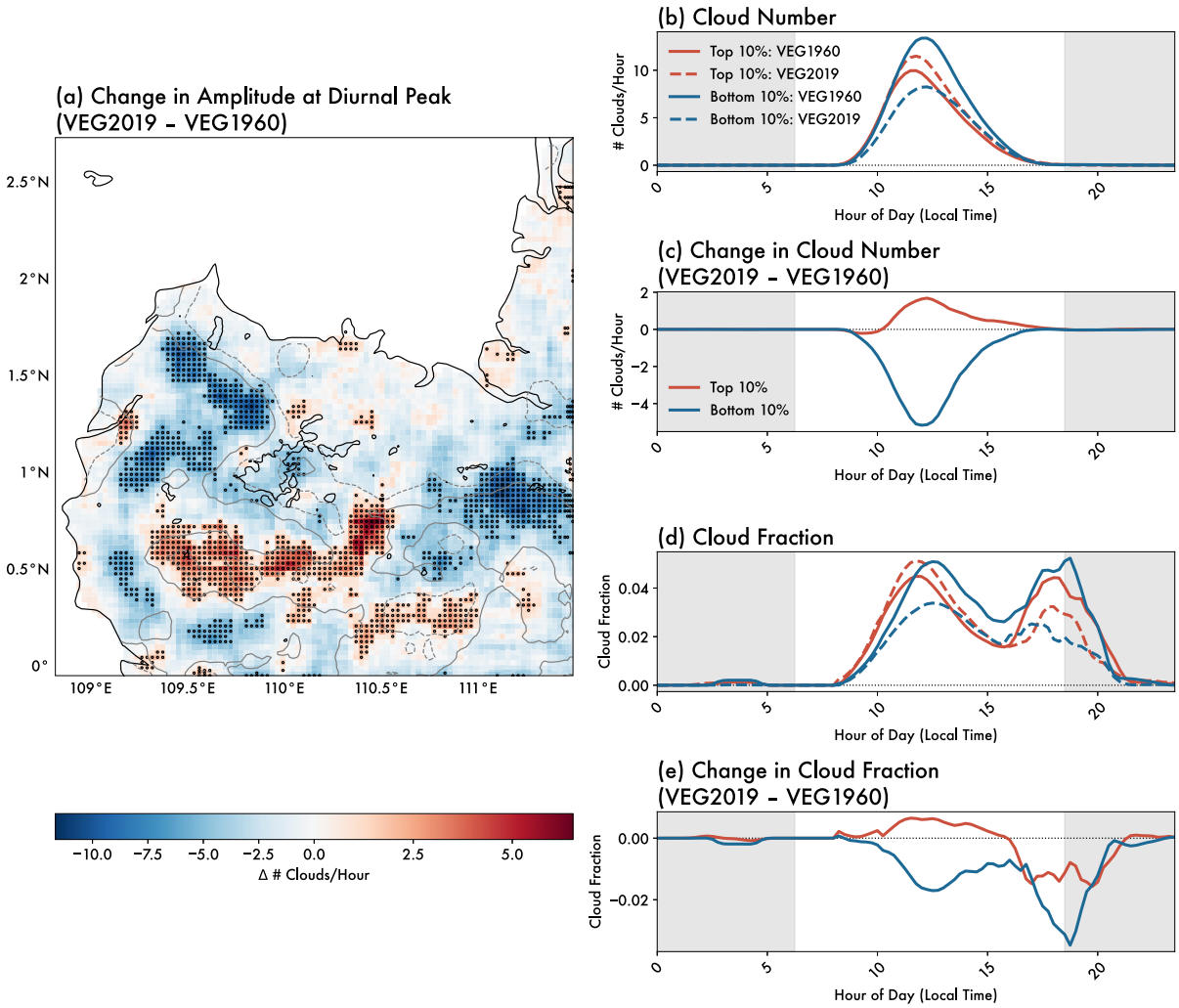

Figure 7. Spatial heterogeneity in cloud response to deforestation. (a) Difference in the amplitude of the diurnal peak in cloud formation between VEG2019 and VEG1960, as described in the text. Gray contours show 25% (dashed) and 50% (solid) forest loss between VEG1960 and VEG2019. Black contours show coastline and 500 m a.s.l. Circles represent top (red) and bottom (blue) decile of points in terms of the change in the cloud diurnal peak, used for averaging in (b–e). Mean diurnal cycle of cloud (b) number and (d) fraction are shown for the top/bottom decile of all land grid points, with the VEG1960 simulation in solid lines and the VEG2019 simulation in dashed lines. Changes shown VEG2019-VEG1960 for cloud (c) number and (d) fraction.

The spatial pattern of deforestation-induced cloud changes comprises dipole structures of cloudiness aligned along regions of forest loss from VEG1960 to VEG2019. Regions where cloudiness is enhanced tend to be located on the side of the deforestation boundary with less forest loss, suggesting anomalous mesoscale circulations. Figure 8 shows regions of enhanced cloudiness coincide with areas where turbulent heat fluxes and near-surface virtual potential temperature are locally enhanced. Vertical cross-sections of the flow (Figure 8d; see Figures S3–S5 in Supporting Information S1 for additional cross-sections) show that in regions with a strong spatial gradient in forest loss (Figure 8f), the resulting SHF gradient (Figure 8e) drives a solenoidal circulation with the ascending branch on the warmer, drier, and less deforested side of the gradient. These mesoscale circulations—referred to as vegetation breezes (J. Chen et al., 2023; Khanna et al., 2017; Saad et al., 2010)—transport low-level moist air from more deforested regions (where LHFs are higher) to less deforested regions where air is more buoyant. These anomalous circulations provide the lift for cloud formation, and drive local increases in forced cumuli along the deforestation boundary (Ascher et al., 2025; Falk et al., 2025).

Where deforestation is more spatially uniform (e.g., northwestern coast), we do not find evidence for strengthened mesoscale circulations with deforestation (Figure S6 in Supporting Information S1). Instead, diurnal peak cloudiness decreases (Figure 7a) along with a decrease in low-level buoyancy (Figure 8b), reflecting the domain-

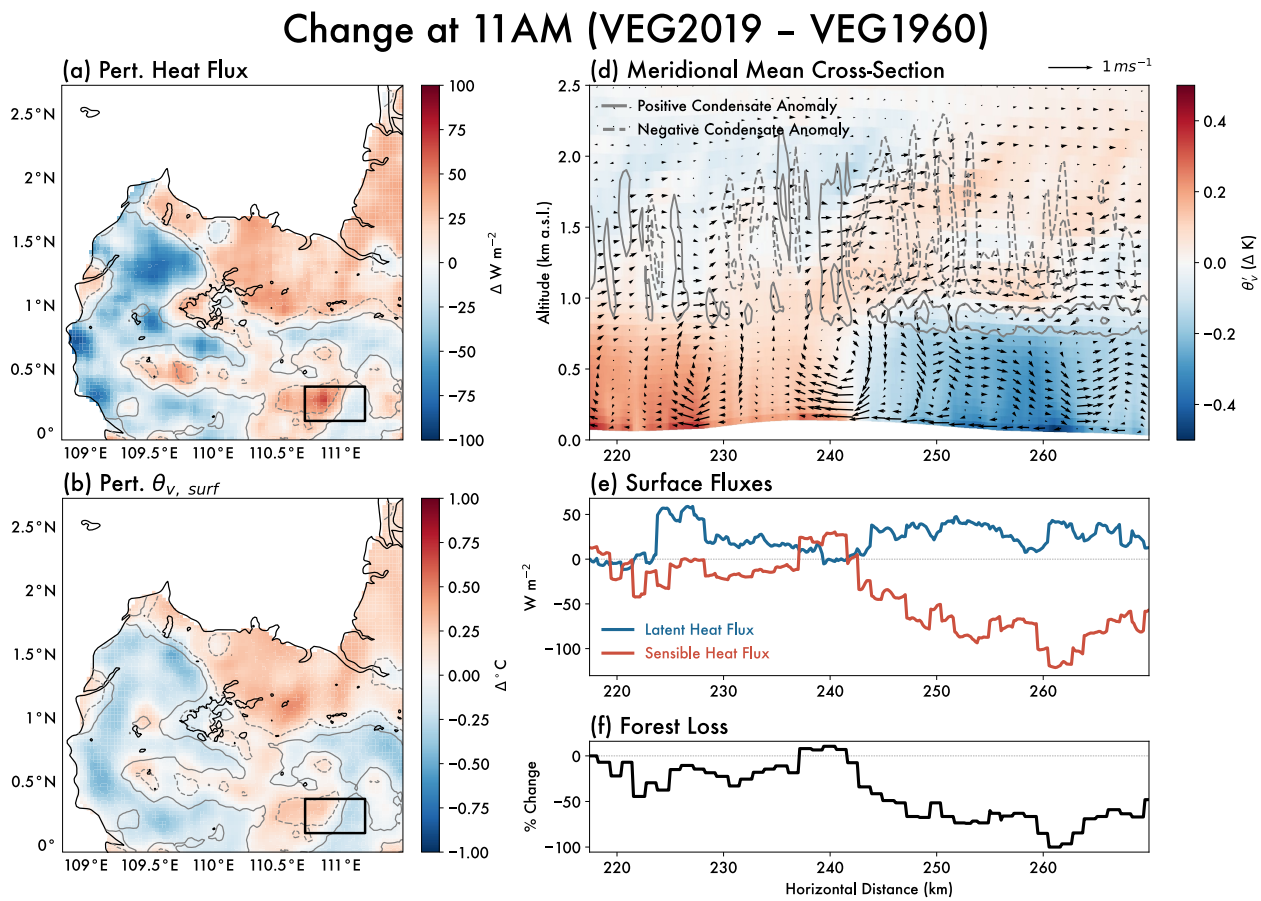

Figure 8. Mesoscale solenoidal circulations are driven by gradients in surface heat flux and buoyancy. Maps of the change (VEG2019−VEG1960) in perturbation (a) surface heat flux (sensible + latent) and (b) virtual potential temperature at 75 m a.g.l. (perturbation from spatiotemporal mean for given hour) from 10:30–11:30a.m., prior to the peak in daytime convection. Black box (a, b) shows the region in vertical cross-section (d–f), averaged meridionally. Panel (d) shows the change in the zonally averaged cross-section of virtual potential temperature perturbation (color shading), meridional and vertical winds (black arrows; vertical winds scaled by 5 to highlight vertical motion), and cloud condensate (gray contours; dashed lines are decrease in condensate and solid lines are increase in condensate, at intervals of 0.005 g kg^{-1}). Panel (e) shows the corresponding changes in latent (blue) and sensible (red) heat fluxes, and (f) shows the change in the percent of land area covered by forested land.

mean response to deforestation (Figure 5). This highlights the importance of the spatial pattern of deforestation in determining whether mesoscale circulations favoring convection can overcome the mean thermodynamics hindering convection at any given location.

4.4. Impacts on Sea Breeze and Deep Convection

Across the domain, there is a reduction in deep convection following deforestation (Figures 5b and 5d). First, we explore whether this is merely due to reduced shallow cumuli earlier in the day (Section 4.1). We calculated the relative contribution of the congestus and deep convective modes in the evening (4–8p.m, peak deep convective activity) from Figure 5d. In VEG2019, terminal congestus (those do not grow to become deep convection later) contribute a 10% larger share of cloudy area when compared to VEG1960. This suggests that even when clouds do form in VEG2019, they are less likely to develop into deep convection compared with VEG1960.

We investigate the causes of this difference in the shallow-to-deep convective transition, and find substantial differences in the large-scale moisture convergence associated with the sea breeze. The SSTs in the two simulations are nearly identical. However, there is a near-surface cooling over land in VEG2019, which leads to a weakening of the sea breeze compared to VEG1960. Figure 9 shows the low-level moisture flux convergence (MFC; vertically integrated from the surface to 1 km a.g.l) averaged over land as a function of distance from the nearest coastline. The sea breeze does not penetrate as far inland (~2 km closer to the coastline) and generally

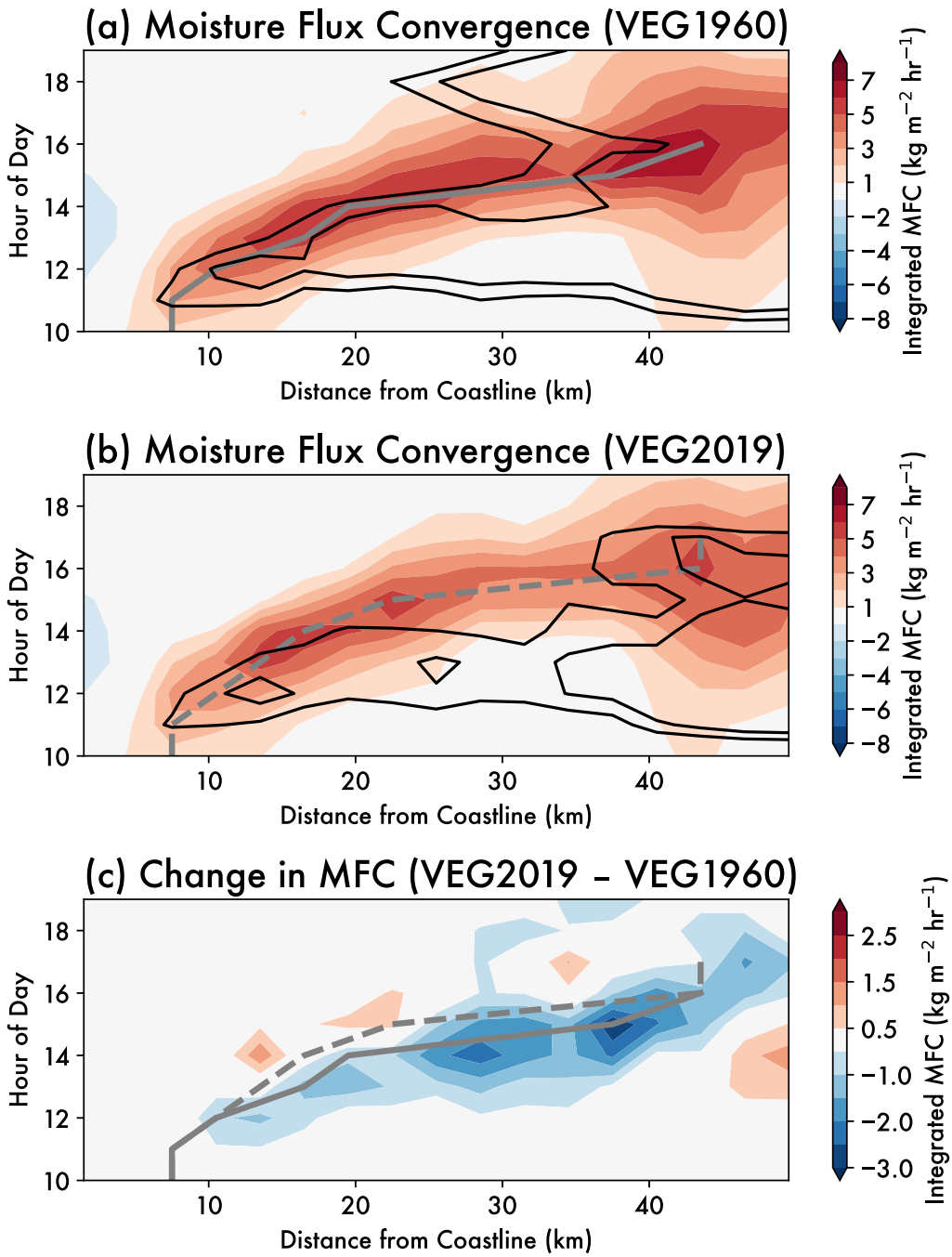

Figure 9. Hovmöller plot showing sea breeze propagation and associated moisture flux convergence (MFC) and cloud cover for (a) VEG1960, (b) VEG2019, and (c) the difference between VEG2019 and VEG1960. Color shading (a, b) shows integrated MFC (surface–1 km a.g.l.), as a function of distance from the coastline and hour of the day. Black contours show a cloud fraction of 3% and 3.5%. Gray lines show the location of peak MFC for each time in VEG1960 (solid) and VEG2019 (dashed).

fluxes less moisture inland (maximum MFC is ∼1 kg m^{-2} hr^{-1} lower) following deforestation. This is consistent with past research on surface roughness and evapotranspiration impacts on sea breeze strength and propagation (Gero & Pitman, 2006; Grant & van den Heever, 2014).

As a result of the reduced onshore moisture flux following deforestation, fewer deep convective cells initiate in the late afternoon (Figure 5d) along the sea breeze front (black contours; Figures 9a and 9b) in VEG2019

compared with VEG1960. Also, the development of the fewer deep convective clouds in VEG2019 is shifted to later in the evening (Figure 7c).

5. Implications for Precipitation

The changes in convection across the diurnal cycle caused by widespread deforestation have substantial implications for surface precipitation. Figure 10 shows changes in the diurnal cycle of clouds across the domain, as in Figure 7, but only for clouds with appreciable surface rainfall (rain rate >0.01 mm hr^{-1}). The area with positive changes (i.e., more raining clouds) is more evenly distributed across Figure 10a compared to Figure 7a. Although mesoscale circulations support increased convection along the deforestation boundary, the change in *raining* cumuli is more spatially uniform. This suggests the increase in shallow cumulus rainfall is driven by domain-wide changes in low-level moisture rather than lifting driven by surface heterogeneities, though these may still play a secondary role. Fewer active shallow cumuli form in VEG2019, but those which do have access to more near-surface moisture and trigger the onset of precipitation earlier in the day (Figures 10b, 10c and 11a, 11c). Although these precipitating shallow cumuli comprise a small number and a limited integrated contribution to the overall water budget, these deforestation-driven changes happen during a time of day when little precipitation generally occurs. Thus, any shifts have a large relative contribution to when and where rainfall occurs (8% increase in raining area and 20% increase in rain amount from shallow cumuli between 9a.m. and 3p.m.).

In contrast to the aforementioned changes in rainfall from shallow cumulus, we find that deforestation suppresses deep convection associated with sea breeze convergence, thereby leading to a decrease in the magnitude of the diurnal rainfall peak (Figure 11d). The majority of rainfall is driven by deep convection that forms after 3 p.m. (Figure 11b), and thus the net deforestation impact is a decrease in overall precipitation.

6. Conclusions

Accelerating deforestation in many regions of the world, including Southeast Asia, motivates an urgent need to understand the impact such land cover changes have on clouds and precipitation. Global and regional climate models disagree about the sign of deforestation-induced cloud feedbacks, which demonstrates a gap in our understanding of the convective and mesoscale processes involved. In this study, we use a set of high-resolution large eddy simulations with varied land cover but identical atmospheric initial and boundary conditions to elucidate the mechanisms by which deforestation impacts clouds over Borneo on daily timescales. We focus on how land surface–convection interactions are influenced by changes in mean thermodynamics and mesoscale features such as vegetation and sea breezes. Figure 12 illustrates the processes governing these interactions.

Overall, we find that deforestation induces robust changes in the surface energy budget and thermodynamic responses in the near-surface atmosphere. The shift from rainforest to palm and rubber plantations reduces surface roughness and makes turbulent land-atmosphere exchanges less efficient. This leads to a decrease in sensible heat fluxes that is primarily compensated for by added energy storage in the ground and vegetation canopy, leading to warmer ground surface temperatures. Unlike in other regions where the conversion of forest to pasture or bare soil decreases latent heat fluxes, we find that under these moisture-rich conditions deforestation enhances afternoon evapotranspiration in response to greater canopy heating and weaker evaporative resistance. This unique surface response is consistent with in situ observations (Fowler et al., 2011; Giambelluca et al., 2016). However, regional and global climate modeling studies for this region have often found the opposite, with deforestation leading to decreased latent heat fluxes and low-level drying (Takahashi et al., 2017; Tölle et al., 2017) or increased moisture arising through a different pathway involving enhanced low-level moisture convergence (C.-C. Chen et al., 2019). It remains unclear whether these discrepancies arise from unique feedbacks that require that shallow cumulus be sufficiently resolved, transient differences in the surface fluxes as soil moisture equilibrates, structural differences between models, or background meteorology (H. Chen & Lo, 2023). We suspect all of the above factors could likely contribute and suggest investigating differences in cloud responses to deforestation between models across scalesis worth further study. It would be valuable to assess whether these convective responses on short timescales are present in longer-term climate simulations run at similar cumulus-resolving grid scales.

We find that the aforementioned changes to the surface energy budget lead to a cooler and moister near-surface atmosphere following widespread deforestation. That being said, we find deforestation impacts on clouds are not homogeneous: changes vary spatially and diurnally. Deforestation drives a decrease in late morning cloudiness across the region via reduced sensible heat fluxes and enhanced convective inhibition. Yet shallow cloudiness can

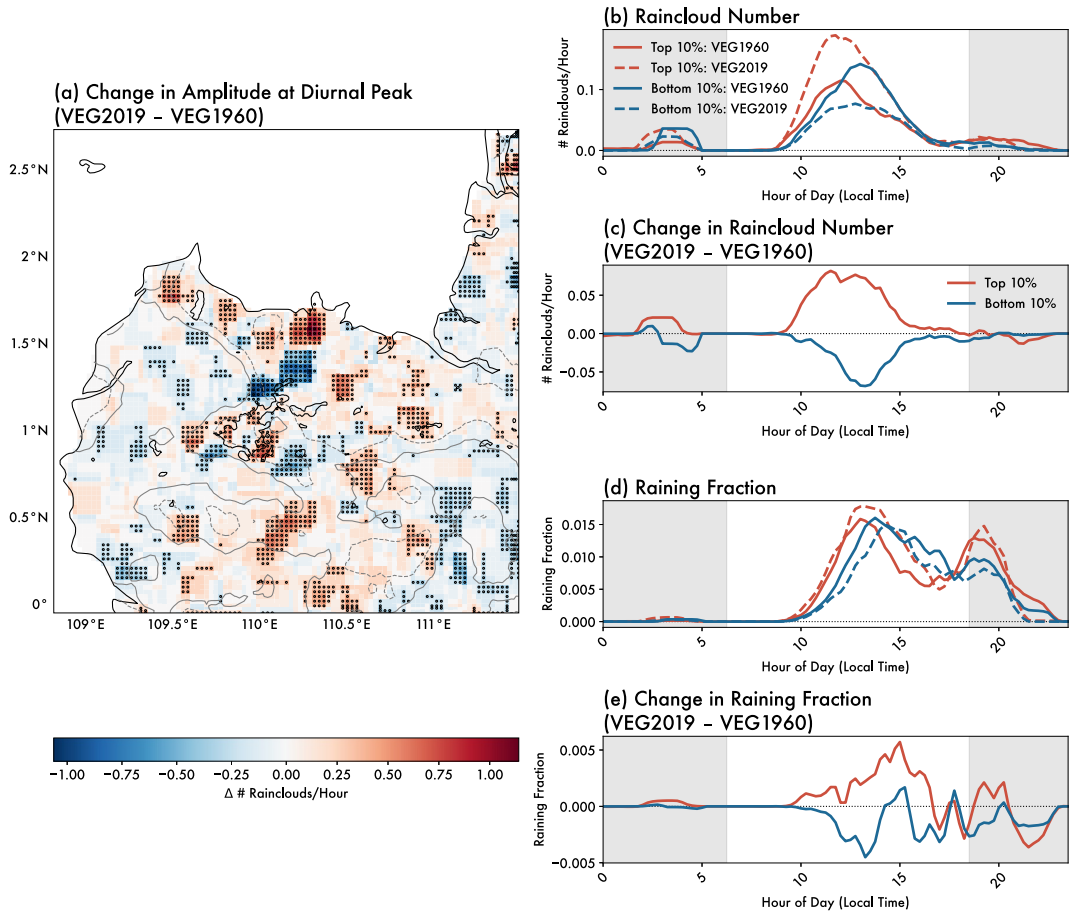

Figure 10. Spatial heterogeneity in raining cloud response to deforestation. As in Figure 7, but only for precipitating clouds (rain rate >0.01 mm hr^{-1}).

be locally enhanced by vegetation breezes around areas with substantial forest loss. Crucially, we find the degree of deforestation heterogeneity mediates the competition between regional and local responses. The spatial pattern of deforestation determines whether mesoscale circulations that support convection can overcome the mean thermodynamic changes that suppress them. Quantifying the net deforestation impact on shallow clouds—which have strong radiative implications for climate—thus depends on the spatial pattern of deforestation and the degree of land surface heterogeneity.

Furthermore, we find that despite this region-wide suppression of shallow cumuli, the increased low-level moisture drives more of the shallow cumuli that do form to start raining earlier in the day. This leads to shifts in the diurnal timing and coverage of shallow precipitation, which motivates the need for further observational validation that disaggregates deforestation impacts on clouds and rainfall at different times of day (Leung et al., 2024; Ruijsch et al., 2025).

Deep convection is strongly impacted by deforestation-induced changes in large-scale moisture flux convergence. Deforestation dampens the land-ocean contrast in low-level temperatures, thereby weakening the sea breeze. This reduces moisture advection and limits convective development, resulting in proportionally more clouds remaining as congestus (4 km < CTH < 10 km) rather than deep convection (CTH > 10 km). The deep convection that does develop under the deforested scenario tends to occur beyond sunset, with corresponding shifts in the diurnal precipitation maxima. Changes in diurnal timing may impact the net radiative effects of deep convective clouds and their anvils (Jones et al., 2024).

Compared to better-studied deforestation hotspots like the Amazon, the region of Southeast Asia we focus on here is unique both in terms of the prevailing land use (with the transition to oil palm and rubber plantations meaning

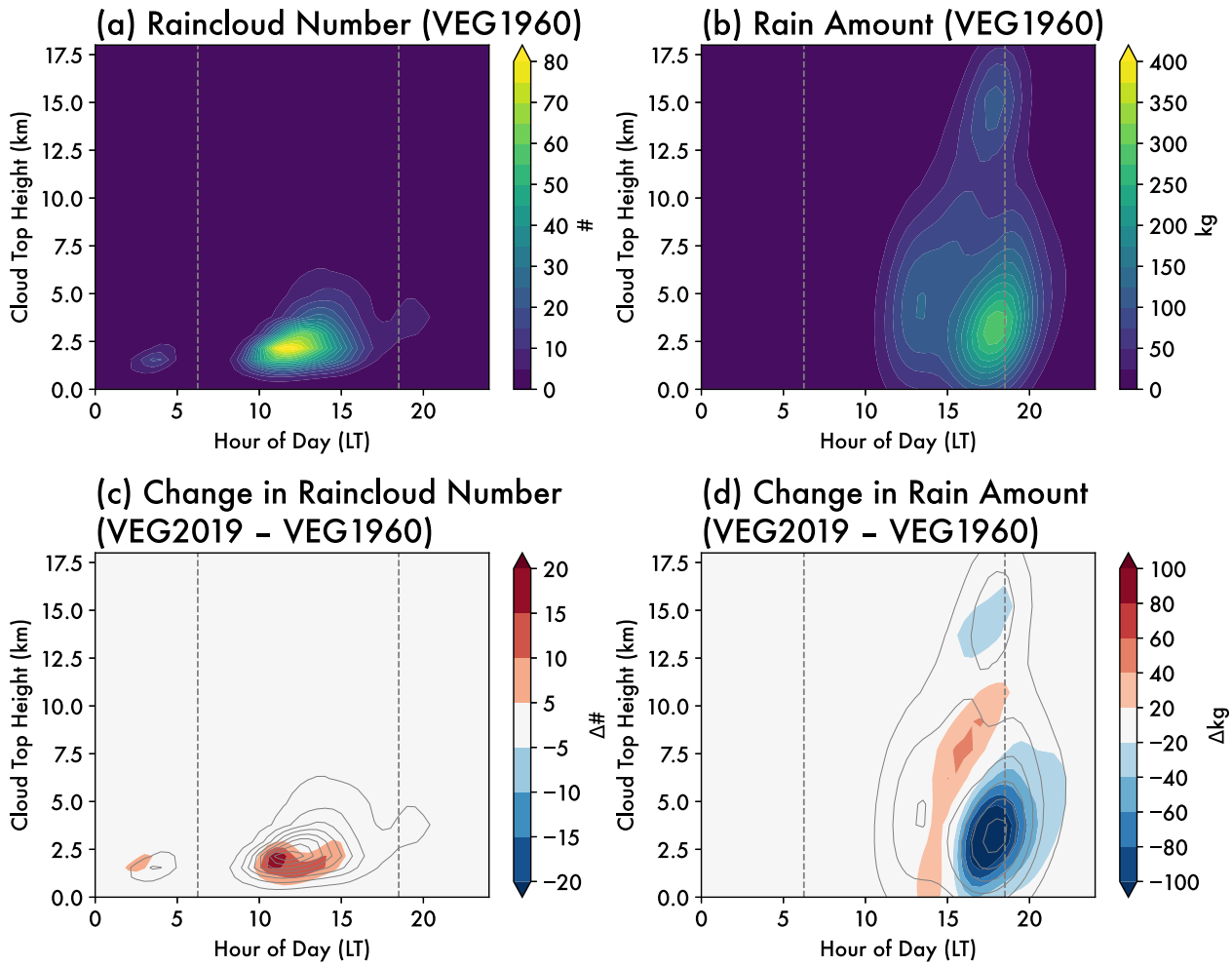

Figure 11. Diurnal cycle of (a) number of raining clouds and (b) total rain amount. As in Figure 5, but only for precipitating clouds (rain rate >0.01 mm hr^{-1}). Total rain amount (b, d) is integrated over cloud area and summed for each (time-of-day, CTH) bin.

evapotranspiration remains relatively high) and background meteorology (highly moist, with strong mesoscale influences on convection). We speculate the processes discussed here are broadly applicable to other tropical deforestation regions with nearby moisture sources (e.g., Central America, coastal West Africa) (Kim et al., 2015; Taylor et al., 2022). That said, the *net* deforestation response is highly dependent on relative contributions from the local and regional processes we elucidate in this paper and thus may vary across regions and even seasons. For example, mesoscale breezes might become relatively more important compared to regional mean changes in boundary layer cloud development during the dry season (Leung et al., 2024). Large-scale climate variability and its controls on the background meteorological conditions are likely also an important control for the overall sign and magnitude of deforestation impacts on convection (Lee & Lo, 2021). Deforestation impacts may further be modulated by other properties such as aerosol emissions from forest clearing-related biomass burning (as visible in smoke in Figures 1a and 1d, not included in our simulations). Such aerosol–land surface–cloud feedbacks can impact mesoscale circulations like sea breezes (Grant & van den Heever, 2014; Park & van den Heever 2022) and are the subject of future planned investigations.

In conclusion, we demonstrate that shallow and deep convection are coupled to the land surface through different spatiotemporal scales. Shallow convection is more sensitive to deforestation-induced regional changes in thermodynamics and local changes in vegetation breezes, whereas deep convection is more sensitive to changes in moisture convergence associated with the sea breeze. There are strong diurnal structures and mesoscale heterogeneities in the signal of deforestation-driven changes in clouds and precipitation. Although this study focuses on convective-scale adjustments to deforestation and not the equilibrium climate response, it remains uncertain to

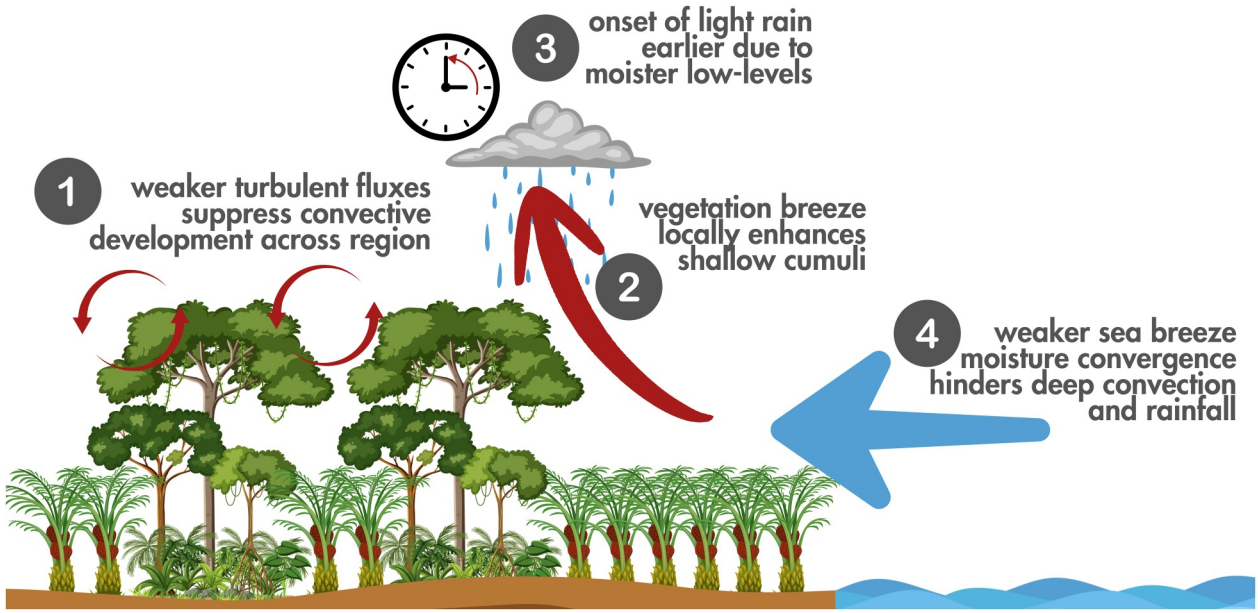

Figure 12. Schematic of processes impacting the cloud response to deforestation over Borneo. As tropical rainforests are replaced by palm oil plantations, turbulent exchange between land and atmosphere is reduced which suppresses convective development overall (1). Along the border of deforested areas, vegetation breezes locally enhance midday shallow cumuli (2). Due to the moister low-level atmosphere, shallow cumuli which do form after deforestation tend to rain earlier in the day (3). The large-scale changes in the near-surface atmosphere over land weaken moisture flux convergence by the sea breeze, hindering the development of deep convection in the evening (4).

what extent these adjustments impact the net response in large-scale models that do not resolve these processes. Our findings emphasize that these convective and mesoscale processes must be carefully incorporated into assessments of the impacts of land cover changes on clouds, hydrology, and climate.

Conflict of Interest

The authors declare no conflicts of interest relevant to this study.

Availability Statement

Source code to reproduce the RAMS simulations is available at https://doi.org/10.5281/zenodo.17055884 (Leung & van den Heever, 2025a). Analysis and plotting code are available at https://doi.org/10.5281/zenodo.17122475 (Leung & van den Heever, 2025b).

Acknowledgments
Funding was provided by NASA Early Career Research (FINESST 80NSSC22K1446). SCvdH acknowledges funding from NSF ESCAPE 2019947 and DOE TRACER DE-SC0021160. Computing resources were provided by NASA High-End Computing through the NASA Advanced Supercomputing Division at the Ames Research Center. We thank Dr. Aryeh Drager and Dr. Adele Igel for discussions on surface and radiation parameterizations. We thank two anonymous reviewers for their helpful comments.

References

Argüeso, D., Romero, R., & Homar, V. (2020). Precipitation features of the maritime continent in parameterized and explicit convection models. https://doi.org/10.1175/JCLI-D-19-0416.1

Ascher, B. D., Saleeby, S. M., Marinescu, P. J., & van den Heever, S. C. (2025). Forest breeze–cold pool interactions drive convective organization over heterogeneous vegetation. https://doi.org/10.1175/JAS-D-24-0084.1

Baidya Roy, S., & Avissar, R. (2002). Impact of land use/land cover change on regional hydrometeorology in Amazonia. *Journal of Geophysical Research*, *107*(D20), 1–12. https://doi.org/10.1029/2000JD000266

Boysen, L. R., Brovkin, V., Pongratz, J., Lawrence, D. M., Lawrence, P., Vuichard, N., et al. (2020). Global climate response to idealized deforestation in CMIP6 models. *Biogeosciences*, *17*(22), 5615–5638. https://doi.org/10.5194/bg-17-5615-2020

Chen, C.-C., Lo, M.-H., Im, E.-S., Yu, J.-Y., Liang, Y.-C., Chen, W.-T., et al. (2019). Thermodynamic and dynamic responses to deforestation in the maritime continent: A modeling study. *Journal of Climate*, *32*(12), 3505–3527. https://doi.org/10.1175/JCLI-D-18-0310.1

Chen, H., & Lo, M. (2023). Contrasting responses of surface heat fluxes to tropical deforestation. *Journal of Geophysical Research: Atmospheres*, *128*(12), e2022JD038118. https://doi.org/10.1029/2022JD038118

Chen, J., Hagos, S., Xiao, H., Fast, J., & Feng, Z. (2023). Multiscale analysis of surface heterogeneity–induced convection on isentropic coordinates. https://doi.org/10.1175/JAS-D-21-0198.1

Chen, S., Woodcock, C., Dong, L., Tarrio, K., Mohammadi, D., & Olofsson, P. (2024). Review of drivers of forest degradation and deforestation in Southeast Asia. *Remote Sensing Applications: Society and Environment*, *33*, 101129. https://doi.org/10.1016/j.rsase.2023.101129

Cioni, G., & Hohenegger, C. (2017). Effect of soil moisture on diurnal convection and precipitation in large-eddy simulations. *Journal of Hydrometeorology*, *18*(7), 1885–1903. https://doi.org/10.1175/JHM-D-16-0241.1

Cotton, W. R., Pielke, S. R. A., Walko, R. L., Liston, G. E., Tremback, C. J., Jiang, H., et al. (2003). RAMS 2001: Current status and future directions. *Meteorology and Atmospheric Physics*, *82*(1), 5–29. https://doi.org/10.1007/s00703-001-0584-9

Crompton, O., Corrêa, D., Duncan, J., & Thompson, S. (2021). Deforestation-induced surface warming is influenced by the fragmentation and spatial extent of forest loss in maritime Southeast Asia. *Environmental Research Letters*, *16*(11), 114018. https://doi.org/10.1088/1748-9326/ac2fdc

Davin, E. L., & de Noblet-Ducoudré, N. (2010). Climatic impact of global-scale deforestation: Radiative versus nonradiative processes. *Journal of Climate*, *23*(1), 97–112. https://doi.org/10.1175/2009JCLI3102.1

Duveiller, G., Filipponi, F., Ceglar, A., Bojanowski, J., Alkama, R., & Cescatti, A. (2021). Revealing the widespread potential of forests to increase low level cloud cover. *Nature Communications*, *12*(1), 4337. https://doi.org/10.1038/s41467-021-24551-5

Falk, N. M., Leung, G. R., Grant, L. D., & van den Heever, S. C. (2025). Cold pools reduce the impacts of deforestation on convective initiation.

FAO United Nations. (1974). *Soil map of the world*. Unesco.

Findell, K. L., & Eltahir, E. A. B. (2003). Atmospheric controls on soil moisture–boundary layer interactions. Part I: Framework development. *Journal of Hydrometeorology*, *4*(3), 552–569. https://doi.org/10.1175/1525-7541(2003)004<0552:ACOSML>2.0.CO;2

Fowler, D., Nemitz, E., Misztal, P., Di Marco, C., Skiba, U., Ryder, J., et al. (2011). Effects of land use on surface–atmosphere exchanges of trace gases and energy in Borneo: Comparing fluxes over oil palm plantations and a rainforest. *Philosophical Transactions of the Royal Society B: Biological Sciences*, *366*(1582), 3196–3209. https://doi.org/10.1098/rstb.2011.0055

Friedl, M. A., McIver, D. K., Hodges, J. C. F., Zhang, X. Y., Muchoney, D., Strahler, A. H., et al. (2002). Global land cover mapping from MODIS: Algorithms and early results. *Remote Sensing of Environment*, *83*(1), 287–302. https://doi.org/10.1016/S0034-4257(02)00078-0

Gentine, P., Holtslag, A. A. M., D'Andrea, F., & Ek, M. (2013). Surface and atmospheric controls on the onset of moist convection over land. *Journal of Hydrometeorology*, *14*(5), 1443–1462. https://doi.org/10.1175/JHM-D-12-0137.1

Gentine, P., Massmann, A., Lintner, B. R., Hamed Alemohammad, S., Fu, R., Green, J. K., et al. (2019). Land–atmosphere interactions in the tropics – A review. *Hydrology and Earth System Sciences*, *23*(10), 4171–4197. https://doi.org/10.5194/hess-23-4171-2019

Gero, A. F., & Pitman, A. J. (2006). The impact of land cover change on a simulated storm event in the Sydney Basin. *Journal of Applied Meteorology and Climatology*, *45*(2), 283–300. https://doi.org/10.1175/JAM2337.1

Giambelluca, T. W., Mudd, R. G., Liu, W., Ziegler, A. D., Kobayashi, N., Kumagai, T., et al. (2016). Evapotranspiration of rubber (Hevea brasiliensis) cultivated at two plantation sites in Southeast Asia. *Water Resources Research*, *52*(2), 660–679. https://doi.org/10.1002/2015WR017755

Grant, L. D., & van den Heever, S. C. (2014). Aerosol-cloud-land surface interactions within tropical sea breeze convection. *Journal of Geophysical Research: Atmospheres*, *119*(13), 8340–8361. https://doi.org/10.1002/2014JD021912

Hardwick, S. R., Toumi, R., Pfeifer, M., Turner, E. C., Nilus, R., & Ewers, R. M. (2015). The relationship between leaf area index and microclimate in tropical forest and oil palm plantation: Forest disturbance drives changes in microclimate. *Agricultural and Forest Meteorology*, *201*, 187–195. https://doi.org/10.1016/j.agrformet.2014.11.010

Heikenfeld, M., Marinescu, P. J., Christensen, M., Watson-Parris, D., Senf, F., van den Heever, S. C., & Stier, P. (2019). Tobac 1.2: Towards a flexible framework for tracking and analysis of clouds in diverse data sets. *Geoscientific Model Development*, *12*(11), 4551–4570. https://doi.org/10.5194/gmd-12-4551-2019

Hersbach, H., Bell, B., Berrisford, P., Hirahara, S., Horányi, A., Muñoz-Sabater, J., et al. (2020). The ERA5 global reanalysis. *Quarterly Journal of the Royal Meteorological Society*, *146*(730), 1999–2049. https://doi.org/10.1002/qj.3803

Hill, G. E. (1974). Factors controlling the size and spacing of cumulus clouds as revealed by numerical experiments. Retrieved from https://journals.ametsoc.org/view/journals/atsc/31/3/1520-0469_1974_031_0646_fctsas_2_0_co_2.xml

Jamaludin, J., De Alban, J. D. T., Carrasco, L. R., & Webb, E. L. (2022). Spatiotemporal analysis of deforestation patterns and drivers reveals emergent threats to tropical forest landscapes. *Environmental Research Letters*, *17*(5), 054046. https://doi.org/10.1088/1748-9326/ac68fa

Johnson, R. H., Rickenbach, T. M., Rutledge, S. A., Ciesielski, P. E., & Schubert, W. H. (1999). Trimodal characteristics of tropical convection. *Journal of Climate*, *12*(8), 22–2418. https://doi.org/10.1175/1520-0442(1999)012<2397:tcotc>2.0.co;2

Jones, W. K., Stengel, M., & Stier, P. (2024). A Lagrangian perspective on the lifecycle and cloud radiative effect of deep convective clouds over Africa. *Atmospheric Chemistry and Physics*, *24*(9), 5165–5180. https://doi.org/10.5194/acp-24-5165-2024

June, T., Meijide, A., Stiegler, C., Kusuma, A. P., & Knohl, A. (2018). The influence of surface roughness and turbulence on heat fluxes from an oil palm plantation in Jambi, Indonesia. *IOP Conference Series: Earth and Environmental Science*, *149*(1), 012048. https://doi.org/10.1088/1755-1315/149/1/012048

Khanna, J., Medvigy, D., Fueglistaler, S., & Walko, R. (2017). Regional dry-season climate changes due to three decades of Amazonian deforestation. *Nature Climate Change*, *7*(3), 200–204. https://doi.org/10.1038/nclimate3226

Kim, D.-H., Sexton, J. O., & Townshend, J. R. (2015). Accelerated deforestation in the humid tropics from the 1990s to the 2000s. *Geophysical Research Letters*, *42*(9), 3495–3501. https://doi.org/10.1002/2014GL062777

Laguë, M. M., Swann, A. L. S., & Boos, W. R. (2021). Radiative feedbacks on land surface change and associated tropical precipitation shifts. *Journal of Climate*, *34*(16), 6651–6672. https://doi.org/10.1175/JCLI-D-20-0883.1

Lee, T.-H., & Lo, M.-H. (2021). The role of El Niño in modulating the effects of deforestation in the Maritime continent. *Environmental Research Letters*, *16*(5), 054056. https://doi.org/10.1088/1748-9326/abe88e

Leung, G. R., Grant, L. D., & van den Heever, S. C. (2024). Deforestation-driven increases in shallow clouds are greatest in drier, low-aerosol regions of Southeast Asia. *Geophysical Research Letters*, *51*(10), e2023GL107678. https://doi.org/10.1029/2023GL107678

Leung, G. R., & van den Heever, S. C. (2022). Controls on the development and circulation of terminal versus transient congestus clouds and implications for midlevel aerosol transport. *Journal of the Atmospheric Sciences*, *79*(11), 3083–3101. https://doi.org/10.1175/JAS-D-21-0314.1

Leung, G. R., & van den Heever, S. C. (2025). Grleung/borneolcc: Code associated with Leung and van den Heever (2025) (version v1.0-jgra) [Software]. *Zenodo*. Retrieved from https://zenodo.org/records/17122476

Leung, G. R., & van den Heever, S. C. (2025). Grleung/rams: RAMS Borneo LCC simulations (version borneolcc-paper) [Software]. *Zenodo*. https://doi.org/10.5281/zenodo.17055884

Lilly, D. K. (1962). On the numerical simulation of buoyant convection. *Tellus*, *14*(2), 148–172. https://doi.org/10.1111/j.2153-3490.1962.tb00128.x

Luo, Z., Liu, G. Y., Stephens, G. L., & Johnson, R. H. (2009). Terminal versus transient cumulus congestus: A CloudSat perspective. *Geophysical Research Letters*, *36*(5). https://doi.org/10.1029/2008GL036927

Mahmood, R., Pielke, S. R. A., Hubbard, K. G., Niyogi, D., Dirmeyer, P. A., McAlpine, C., et al. (2014). Land cover changes and their biogeophysical effects on climate. *International Journal of Climatology*, *34*(4), 929–953. https://doi.org/10.1002/joc.3736

Marzuki, M., Yusnaini, H., Ramadhan, R., Tangang, F., Amirudin, A. A. B., Hashiguchi, H., et al. (2022). Characteristics of precipitation diurnal cycle over a mountainous area of Sumatra island including MJO and seasonal signatures based on the 15-Year optical rain gauge data, WRF model and IMERG. *Atmosphere*, *13*(1), 63. https://doi.org/10.3390/atmos13010063

Meyers, M. P., Walko, R. L., Harrington, J. Y., & Cotton, W. R. (1997). New RAMS cloud microphysics parameterization. Part II: The two-moment scheme. *Atmospheric Research*, *45*(1), 3–39. https://doi.org/10.1016/S0169-8095(97)00018-5

Park, J. M. , & van den Heever, S. C. (2022). Weakening of tropical sea breeze convective systems through interactions of aerosol, radiation, and soil moisture. *Atmospheric Chemistry and Physics*, *22*(16), 10527–10549. https://doi.org/10.5194/acp-22-10527-2022

Parker, D., Tosiani, A., Yazid, M., Sari, I. L., Kartika, T., Kustiyo, et al. (2024). Land in limbo: Nearly one third of Indonesia's cleared old-growth forests left idle. *Proceedings of the National Academy of Sciences*, *121*(28), e2318029121. https://doi.org/10.1073/pnas.2318029121

Pielke, S. R. A., Cotton, W. R., Walko, R. L., Tremback, C. J., Lyons, W. A., Grasso, L. D., et al. (1992). A comprehensive meteorological modeling system—rams. *Meteorology and Atmospheric Physics*, *49*(1), 69–91. https://doi.org/10.1007/BF01025401

Pincus, R., Mlawer, E. J., & Delamere, J. S. (2019). Balancing accuracy, efficiency, and flexibility in radiation calculations for dynamical models. *Journal of Advances in Modeling Earth Systems*, *11*(10), 3074–3089. https://doi.org/10.1029/2019MS001621

Qian, J.-H. (2008). Why precipitation is mostly concentrated over Islands in the maritime continent. *Journal of the Atmospheric Sciences*, *65*(4), 1428–1441. https://doi.org/10.1175/2007JAS2422.1

Reid, J. S., Maring, H. B., Narisma, G. T., van den Heever, S., Girolamo, L. D., Ferrare, R., et al. (2023). The coupling between tropical meteorology, aerosol lifecycle, convection, and radiation, during the cloud, aerosol and monsoon processes Philippines experiment (CAMP2Ex). *Bulletin of the American Meteorological Society*, *1*(aop), E1179–E1205. https://doi.org/10.1175/BAMS-D-21-0285.1

Renggono, F., Hashiguchi, H., Fukao, S., Yamanaka, M. D., Ogino, S.-Y., Okamoto, N., et al. (2001). Precipitating clouds observed by 1.3-GHz boundary layer radars in equatorial Indonesia. *Annales Geophysicae*, *19*(8), 889–897. https://doi.org/10.5194/angeo-19-889-2001

Rieck, M., Hohenegger, C., & van Heerwaarden, C. C. (2014). The influence of land surface heterogeneities on cloud size development. *Monthly Weather Review*, *142*(10), 3830–3846. https://doi.org/10.1175/MWR-D-13-00354.1

Ruijsch, J., Taylor, C. M., Hutjes, R. W. A., & Teuling, A. J. (2025). Scale-dependent cloud enhancement from land restoration in West African drylands. *Communications Earth and Environment*, *6*(1), 1–11. https://doi.org/10.1038/s43247-025-02154-y

Saad, S. I., da Rocha, H. R., Dias, M. A. F. S., & Rosolem, R. (2010). Can the deforestation breeze change the rainfall in Amazonia? A case study for the BR-163 highway region. *Earth Interactions*. https://doi.org/10.1175/2010EI351.1

Sabajo, C. R., le Maire, G., June, T., Meijide, A., Roupsard, O., & Knohl, A. (2017). Expansion of oil palm and other cash crops causes an increase of land surface temperature in Indonesia. *Biogeosciences*. https://doi.org/10.5194/bg-2017-203

Saleeby, S. M., & Cotton, W. R. (2008). A binned approach to cloud-droplet riming implemented in a bulk microphysics model. *Journal of Applied Meteorology and Climatology*, *47*(2), 694–703. https://doi.org/10.1175/2007jamc1664.1

Saleeby, S. M., & van den Heever, S. C. (2013). Developments in the CSU-RAMS aerosol model: Emissions, nucleation, regeneration, deposition, and radiation. *Journal of Applied Meteorology and Climatology*, *52*(12), 2601–2622. https://doi.org/10.1175/JAMC-D-12-0312.1

Santanello, J. A., Dirmeyer, P. A., Ferguson, C. R., Findell, K. L., Tawfik, A. B., Berg, A., et al. (2018). Land–atmosphere interactions: The LoCo perspective. *Bulletin of the American Meteorological Society*, *99*(6), 1253–1272. https://doi.org/10.1175/BAMS-D-17-0001.1

Schneck, R., & Mosbrugger, V. (2011). Simulated climate effects of Southeast Asian deforestation: Regional processes and teleconnection mechanisms. *Journal of Geophysical Research*, *116*(D11), D11116. https://doi.org/10.1029/2010JD015450

Smagorinsky, J. (1963). General circulation experiments with the primitive equations. *Monthly Weather Review*. https://doi.org/10.1175/1520-0493(1963)091%3C0099:GCEWTP%3E2.3.CO;2

Sokolowsky, G. A., Freeman, S. W., Jones, W. K., Kukulies, J., Senf, F., Marinescu, P. J., et al. (2024). *Tobac* v1.5: Introducing fast 3D tracking, splits and mergers, and other enhancements for identifying and analysing meteorological phenomena. *Geoscientific Model Development*, *17*(13), 5309–5330. https://doi.org/10.5194/gmd-17-5309-2024

Spracklen, D. V., Baker, J. C. A., Garcia-Carreras, L., & Marsham, J. H. (2018). The effects of tropical vegetation on rainfall. *Annual Review of Environment and Resources*, *43*(1), 193–218. https://doi.org/10.1146/annurev-environ-102017-030136

Stull, R. B. (1988). Boundary layer clouds. In R. B. Stull (Ed.), *An introduction to boundary layer meteorology* (pp. 545–585). Springer Netherlands. https://doi.org/10.1007/978-94-009-3027-8_13

Takahashi, A., Kumagai, T., Kanamori, H., Fujinami, H., Hiyama, T., & Hara, M. (2017). Impact of tropical deforestation and forest degradation on precipitation over Borneo Island. *Journal of Hydrometeorology*, *18*(11), 2907–2922. https://doi.org/10.1175/JHM-D-17-0008.1

Takanashi, S., Kosugi, Y., Ohkubo, S., Matsuo, N., Tani, M., & Nik, A. R. (2010). Water and heat fluxes above a lowland dipterocarp forest in peninsular Malaysia. *Hydrological Processes*, *24*(4), 472–480. https://doi.org/10.1002/hyp.7499

Tang, A. C. I., Stoy, P. C., Hirata, R., Musin, K. K., Aeries, E. B., Wenceslaus, J., et al. (2019). The exchange of water and energy between a tropical peat forest and the atmosphere: Seasonal trends and comparison against other tropical rainforests. *Science of the Total Environment*, *683*, 166–174. https://doi.org/10.1016/j.scitotenv.2019.05.217

Taylor, C. M., Klein, C., Parker, D. J., Gerard, F., Semeena, V. S., Barton, E. J., & Harris, B. L. (2022). "Late-stage" deforestation enhances storm trends in coastal West Africa. *Proceedings of the National Academy of Sciences*, *119*(2), e2109285119. https://doi.org/10.1073/pnas.2109285119

Tölle, M. H., Engler, S., & Panitz, H.-J. (2017). Impact of abrupt land cover changes by tropical deforestation on Southeast Asian climate and agriculture. *Journal of Climate*, *30*(7), 2587–2600. https://doi.org/10.1175/JCLI-D-16-0131.1

van der Molen, M. K., Dolman, A., Waterloo, M., & Bruijnzeel, L. (2006). Climate is affected more by maritime than by continental land use change: A multiple scale analysis. *Global and Planetary Change*, *54*(1–2), 128–149. https://doi.org/10.1016/j.gloplacha.2006.05.005

Walko, R. L., Band, L. E., Baron, J., Kittel, T. G. F., Lammers, R., Lee, T. J., et al. (2000). Coupled atmosphere–biophysics–hydrology models for environmental modeling. *Journal of Applied Meteorology and Climatology*, *39*(6), 931–944. https://doi.org/10.1175/1520-0450(2000)039<0931:cabhmf>2.0.co;2

Werth, D., & Avissar, R. (2005). The local and global effects of Southeast Asian deforestation. *Geophysical Research Letters*, *32*(20). https://doi.org/10.1029/2005GL022970

Winkler, K., Fuchs, R., Rounsevell, M., & Herold, M. (2021). Global land use changes are four times greater than previously estimated. *Nature Communications*, *12*(1), 2501. https://doi.org/10.1038/s41467-021-22702-2

Xu, R., Li, Y., Teuling, A. J., Zhao, L., Spracklen, D. V., Garcia-Carreras, L., et al. (2022). Contrasting impacts of forests on cloud cover based on satellite observations. *Nature Communications*, *13*(1), 670. https://doi.org/10.1038/s41467-022-28161-7

Yang, G.-Y., & Slingo, J. (2001). The diurnal cycle in the tropics. *Monthly Weather Review*. https://doi.org/10.1175/1520-0493(2001)129%3C0784:TDCITT%3E2.0.CO;2